# High-fidelity Simulations of Liquid-gas Colliding Jets Impacted by a Detonation Wave

Ral Bielawski, Supraj Prakash, Venkat Raman
University of Michigan
Ann Arbor, MI, USA

## 1 Introduction

In order to realize detonation-based propulsion devices, it is necessary to understand the role of detonations interacting with liquid droplets. In particular, the reaction structure introduced by this multiphase system will determine the detonation strength and propagation characteristics. Due to the presence of multiple phases and extreme pressure/temperature conditions, numerical simulations remain the best approach to gaining fundamental insight. Here, detailed simulations of a liquid fuel and gaseous oxidizer jet system interacting with a detonation wave are conducted. The focus is on the post-impact structure of the shock wave and the initiation of chemical reactions. Rocket-propellant is used as the fuel. Previous numerical[1, 2, 3, 4] and experimental [5, 6] studies have looked at the canonical shock-tube case of a detonation wave interacting with an oxidizer medium seeded with liquid droplets. Schwer [2] showed qualitative differences when using mono-disperse compared to poly-disperse droplets. Further, it was shown that a minimal droplet size is needed to develop the cellular structure seen in gas-phase detonations. In general, these studies utilize an Eulerian-Lagrangian approach for describing the droplet-gas system [1, 3, 7, 4]. More recently, this approach has been used to study the two-dimensional rotating detonation engine (RDE) configuration [7, 4].

Gas phase simulations of RDEs [8, 9, 10, 11] show that the details of the injection process are critical in determining the detonation characteristics. In particular, the non-homogeneous fuel-air dispersion and mixing alters the local detonation characteristics. As a result, the detonation wave exhibits a thicker internal structure and diminished wave strength and speed [12]. However, similar analysis for liquid-fueled detonations have not been conducted. The focus here is to conduct injection-focused simulations with the goal of understanding detonation propagation over spatially inhomogeneous fuel-air mixtures. A single injection element of a model RDE configuration is used here. The impact of the detonation wave characteristics that impinge on the droplet-laden flow is studied. This work represents some of the first 3D numerical studies of detonations impacting discrete liquid jets for practical hydrocarbons and is a key step for understanding the complex interactions between liquids jets and detonations. The simulation configuration and modeling details are provided in the following section.

## 2 Simulation Configuration

A single liquid-gas injector pair with a channel width of $9.84$ fuel injector diameters ($D$) is utilized as a potential laboratory scale case to study this problem. A narrow channel mimics that found in laboratory-

Correspondence to: rbielaw@umich.edu

Distribution Statement A: Approved for Public Release; Distribution is Unlimited. AFRL-2021-2661.

scale RDEs. A schematic of the computational domain is presented in Fig. 1. Here, a nominal mesh resolution of 200 microns is utilized in the detonation chamber [12, 10].

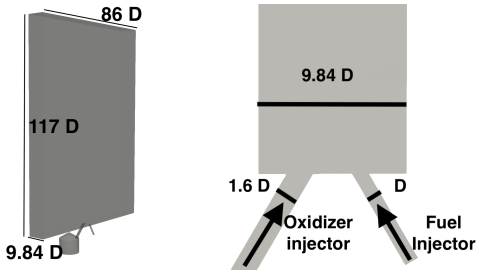


Figure 1: Schematic of the computational domain, where $D$ is the fuel injector diameter.

The oxidizer is gaseous oxygen and the fuel is rocket-propellant (RP) with an equivalence ratio of $1.5$ and total mass flow rate of $3.78\ g/s$. Three different detonations are considered and presented in Tab. 1. For all three cases, detailed chemical kinetics are handled through the HyChem skeletal mechanism for RP [13, 14], consisting of $38$ species and $192$ reactions.

Table 1: Injector mass flow rates and mixture conditions for the three cases.

| Case | Total Mass Flow Rate $(g/s)$ | Equivalence Ratio | Background Mixture |
|---|---|---|---|
| A | 3.78 | 1.5 | RP-O2 $\phi = 0.6$ |
| B | 3.78 | 1.5 | H2-O2 $\phi = 0.25$ |
| C | 3.78 | 1.5 | H2-O2 $\phi = 1.0$ |

The droplets are injected $0.1\ D$ from the exit plane of the fuel injector to reduce the travel time of the droplets, the carrier gas within the injector is RP gas. The droplet size follows a log normal distribution with a mean of $15$ microns and a standard deviation of $10$ microns; the maximum droplet size is limited to four standard deviations from the mean. The initial fill gas in the channel was at atmospheric pressure and $500K$. The flow is allowed to develop for $0.3\ ms$ prior to the introduction of the detonation wave at the left edge of the channel, perpendicular to the injector system.

## 3 Governing Equations

The compressible reactive solver UMReactingFlow was utilized for this problem and has been extensively validated for detonation problems [15]. Two-way mass, momentum and energy coupling is achieved by utilizing UMcloud which solves the Lagrangian transport of droplets. Convective terms are discretized using a Monotonic Upwind Scheme for Conservation Laws-based Harten-Lax-van Leer-Contact approximate Riemann solver. The convective, diffusive and time integration are all discretized to be second-order accurate. Computationally-intensive subroutines for convection and reaction stages are offloaded to the GPU using in-house CUDA-based modules for compatibility with heterogeneous computing platforms. Detailed chemical kinetics and thermodynamic gas properties are evaluated through a matrix-based formulation that maximizes throughput [16], which enables the use of a mechanism with such complexity. The compressible reacting Navier-Stokes equations are presented in detail in Sato et al. [15] and the reader is referred to this work for more details. The gas and liquid phase are coupled through source terms for species mass, momentum and energy transfer added to the gas phase governing equations. The Lagrangian system is governed by the following set of equations:


**Distribution Statement A: Approved for Public Release; Distribution is Unlimited. AFRL-2021-2661.**

$$\begin{aligned}
\frac{d}{dt}\mathbf{x}_p &= \mathbf{u}_p, \\
\frac{d}{dt}\mathbf{u}_p &= \frac{1}{m_p}\sum \mathbf{F}_p, \\
\frac{d}{dt}T_p &= \frac{1}{m_p C_p}E_p, \\
\frac{d}{dt}m_p &= M_p,
\end{aligned} \tag{1}$$

where $\mathbf{x_p}$,$\mathbf{u_p}$, $T_p$, $m_p$, $C_p$ are the droplet position, velocity, temperature, mass and specific heat, respectively. The force ($\mathbf{F_b}$), energy change ($E_p$) and mass change ($M_p$) on the droplet are given by:

$$\begin{aligned}
\mathbf{F}_D &= \frac{m_p Re_p C_{d,p}}{\tau_p}\left(\mathbf{u}_f - \mathbf{u}_p\right), \\
E_p &= hA(T_i - T_c) + Q_{lat}, \\
M_p &= -\pi D Sh \mathcal{D} \rho_v \ln\left(1 + \frac{\chi_{v,s} - \chi_{v,c}}{1 - \chi_{v,s}}\right),
\end{aligned} \tag{2}$$

where, $Re_p$, $C_{d,p}$, $\tau_p$, $\mathbf{u_f}$ are the droplet Reynolds number, drag coefficient, relaxation time, and fluid velocity, respectively. The heat transfer coefficient, droplet area, gas temperature, and latent energy are denoted $h$, $A$, $T_c$, and $Q_{lat}$, respectively. The evaporation parameters: droplet diameter, Sherwood number, mass diffusivity, vapor density, and RP concentration are identified by $D$, $Sh$, $\mathcal{D}$, $\rho_v$, and $\chi$, respectively. The heat transfer coefficient is calculated using a Ranz Marshall model [17] and a Spalding evaporation model is utilized [18]. Droplet break-up is not considered in the current study.

## 4 Results

The results for all three cases will be presented and analyzed. Figure 2 shows snapshots at three instances for case A, including the droplet locations. Prior to detonation, it is seen that droplets impact the oxidizer jet and are dispersed downstream. The larger droplets penetrate further into the oxidizer jet due to their initial momentum. Smaller droplets are accelerated faster by the oxidizer jet and are carried away from the impact location. As the detonation wave passes over the injector, it is seen that the droplets are accelerated by the post-detonation gases in the direction of wave propagation. Moreover, the oxidizer jet becomes unchoked due to the higher pressure in the channel, leading to a drop in mass flow through the oxygen port. At later times, the increased evaporation from the droplets is observed, forming a cloud of fuel vapor near the bottom wall. This behavior, where much of the droplet mass is confined near the bottom wall, will significantly impact detonation propagation. It should be noted that an overdriven, planar detonation wave exists here. Hence, there is no expansion region behind the detonation wave that will restore the injectors to the pre-detonation state. In an RDE, the injectors will reestablish and alter the fuel dispersion characteristics as the pressure recovers. Figure 2 also shows that the number of large droplets is reduced, while the location of the vapor cloud shows a lag between detonation impact and gas-phase fuel generation.

Qualitatively, the detonation results in the droplets being accelerated by the high-speed post-detonation gases, as can be seen in Fig. 3 (right). The droplets that penetrate farthest into the domain are vaporized rapidly with droplets persisting only in regions of high volume fraction. The largest droplets take longer


**Distribution Statement A: Approved for Public Release; Distribution is Unlimited. AFRL-2021-2661.**

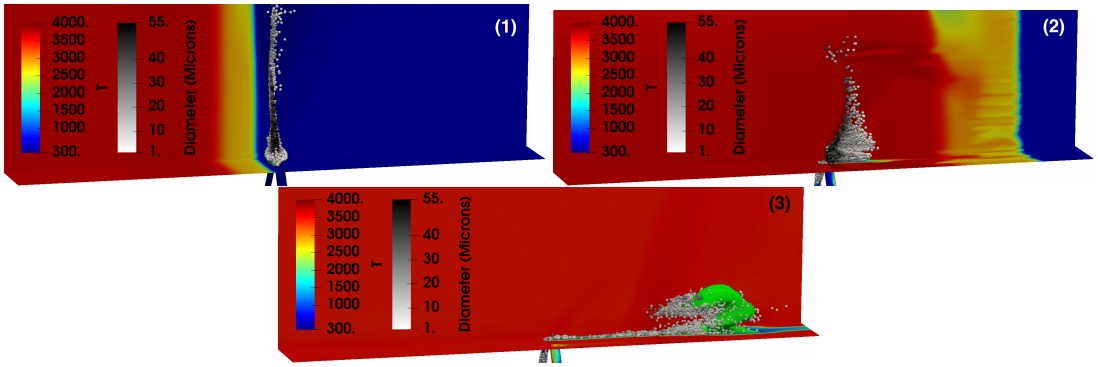


Figure 2: Evolution of the system for case A. The near-wall temperature, droplet diameter and 30% RP mass fraction iso-surface are shown. Image 1 (top left) shows the liquid jet prior to impact, Image 2 (top right) is at 7.2 $\mu$s after impact, and Image 3 (bottom middle) is at 22.2 $\mu$s after impact.

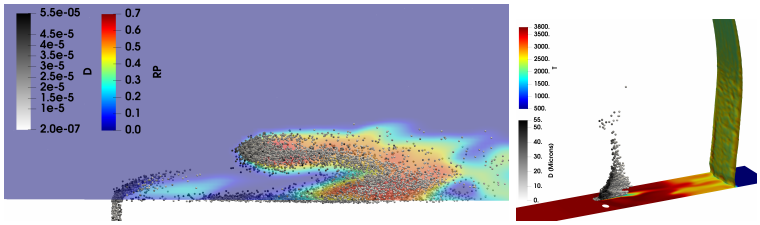


Figure 3: (Left) Post-detonation snapshot showing droplets and gaseous RP due to droplet evaporation for case B. (Right) Droplet spatial distribution and wave location given by the iso-surface of pressure for case A.

to accelerate and create a lower velocity wake. A cluster of small droplets in this wake region is evident in Fig. 3 (left). The reduced-velocity wake shows significant RP mass fraction, as high as 70%, and reactions are stabilized in the shear layer between the high-speed flow and the low-speed wake. All three cases qualitatively show similar behavior.

The heat and mass transfer for all three cases are presented in Fig. 4, where $t = 0$ represents the approximate moment of impact of the detonation with the liquid column, as determined by the instance momentum transfer to the droplets increases. The results for all three cases show a sharp rise in heat and mass transfer when the detonation strikes the liquid jet. The heat transfer peaks with the detonation impact; in cases B and C, the heat transfer begins to decay rapidly after the impact. Case A exhibits a secondary peak in heat transfer before it begins to decay. The mass transfer rate increases as the

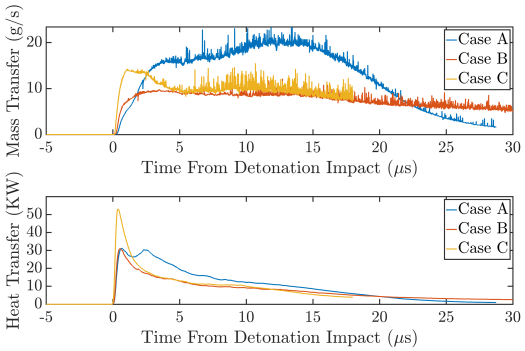


Figure 4: Mass and heat transfer for all three cases between the droplets and gas phase.


**Distribution Statement A: Approved for Public Release; Distribution is Unlimited. AFRL-2021-2661.**

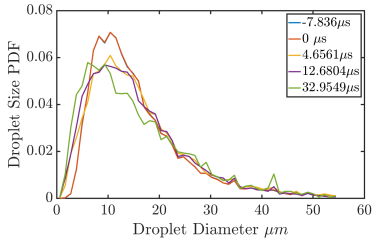


Figure 5: Droplet size distribution for case A where $t = 0$ is the moment the detonation strikes the jet.

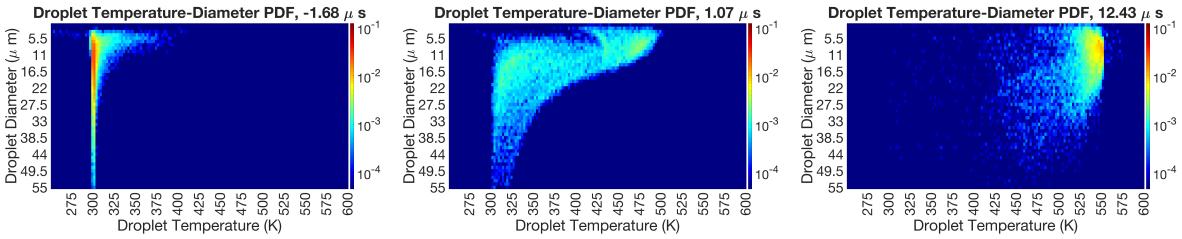


Figure 6: Two-dimensional temperature-diameter probability distributions at three different times for case A. These time represent before, right after, and a long time after the detonation impact.

detonation impacts, with sustained mass transfer in the post detonation region. Case B and C have similar mass transfer rates beyond 5 $\mu$s after detonation, with case C showing a higher peak mass transfer at the time of impact. Case A shows significantly higher mass transfer as the value continues to rise and peaks between $10\mu s$ and $15\mu s$ before rapidly declining. The reason for this difference in mass transfer behavior will be investigated.

The droplet distribution remains constant after the flow develops until the detonation impacts the liquid jet. Following detonation impact, there is a reduction in droplets in the 7-15 micron range, with the probability shifted primarily to smaller droplet sizes, due to evaporation. For case A, the droplet distribution has not recovered by 33 microseconds post-impact. A more detailed look at droplet evolution in time can be seen in the three droplet temperature-diameter distributions shown in Fig. 6. Prior to detonation impact, droplets follow the injected droplet size distribution with only a small percentage of smaller droplets showing any degree of heating. After 1.07 $\mu$s from detonation impact, there is significant heating of droplets with diameter below 19 microns. For droplets larger than 33 microns, there is minimal temperature change with an increase of 50 K or less. The relationship between droplet size and temperature change is believed to be due to the increased thermal mass of larger droplets. After 12.43 $\mu$s from impact, there is significant heating at all droplet diameters with the majority of droplets over $475K$. This delay in heating from the time of impact supports case A's continued increase in mass transfer during the post-detonation period as highlighted in Fig. 4.

## 5 Conclusions

An Eulerian-Lagrangian approach was utilized to perform high-fidelity studies of a detonation wave impacting an injector pair with liquid fuel and gaseous oxidizer in a confined channel. Three different detonation strengths were studied and all three qualitatively showed the same behavior. In each case, the droplets were accelerated downstream with some smaller droplets clustered in the wake of larger droplets and reactions were stabilized at the fringe of the lower velocity wake. Quantitatively, the heat and mass transfer profiles for all the cases were presented. It was found that the post-detonation heat and mass transfer was comparable for the $H_2 - O_2$ detonation waves (case B and C) with case C showing


**Distribution Statement A: Approved for Public Release; Distribution is Unlimited. AFRL-2021-2661.**

a higher heat and mass transfer when the detonation impacted the liquid jet. On the other hand, the $RP - O_2$ (case A) detonation wave demonstrated different behavior in the evolution of mass transfer rate, with sustained increase in evaporative mass transfer following detonation impact. The droplet temperature and diameter evolution was presented for case A, which showed significant heating well into the post-detonation region which reconciles the sustained mass transfer observed for case A.

# References


[1] Douglas A Schwer, Eugene O'Fallon Jr, and David Kessler. *Liquid-Fueled Detonation Modeling at the US Naval Research Laboratory*. Tech. rep. Naval Research Lab Washington DC US, 2018.

[2] Douglas A Schwer. "Multi-dimensional Simulations of Liquid-Fueled JP10/Oxygen Detonations". In: *AIAA Propulsion and Energy 2019 Forum*. 2019, p. 4042.

[3] Zhiwei Huang and Huangwei Zhang. "On the interactions between a propagating shock wave and evaporating water droplets". In: *Physics of Fluids* 32.12 (2020), p. 123315.

[4] Qingyang Meng, Ningbo Zhao, and Huangwei Zhang. "On the distributions of fuel droplets and in situ vapor in rotating detonation combustion with prevaporized n-heptane sprays". In: *Physics of Fluids* 33.4 (2021), p. 043307.

[5] CK Westbrookt and WJ Pitz. "Measurements of cellular structure in spray detonation". In: *Dynamic Aspects of Explosion Phenomena* 154 (1993), p. 148.

[6] KW Ragland, EK Dabora, and JA Nicholls. "Observed structure of spray detonations". In: *The Physics of Fluids* 11.11 (1968), pp. 2377–2388.

[7] Majie Zhao and Huangwei Zhang. "Modelling rotating detonative combustion fueled by partially prevaporized n-heptane sprays". In: *arXiv preprint arXiv:2009.08617* (2020).

[8] Supraj Prakash and Venkat Raman. "The effects of mixture preburning on detonation wave propagation". In: *Proceedings of the Combustion Institute* 38.3 (2021), pp. 3749–3758. ISSN: 1540-7489.

[9] Supraj Prakash et al. "Numerical simulation of a methane-oxygen rotating detonation rocket engine". In: *Proceedings of the Combustion Institute* 38.3 (2021), pp. 3777–3786. ISSN: 1540-7489.

[10] Takuma Sato and Venkat Raman. "Detonation structure in ethylene/air-based non-premixed rotating detonation engine". In: *Journal of Propulsion and Power* 36.5 (2020), pp. 752–762.

[11] Takuma Sato et al. "Mixing and detonation structure in a rotating detonation engine with an axial air inlet". In: *Proceedings of the Combustion Institute* 38.3 (2021), pp. 3769–3776.

[12] Supraj Prakash et al. "Analysis of the detonation wave structure in a linearized rotating detonation engine". In: *AIAA Journal* 58.12 (2020), pp. 5063–5077.

[13] Rui Xu et al. "A physics-based approach to modeling real-fuel combustion chemistry–II. Reaction kinetic models of jet and rocket fuels". In: *Combustion and Flame* 193 (2018), pp. 520–537.

[14] Hai Wang et al. "A physics-based approach to modeling real-fuel combustion chemistry-I. Evidence from experiments, and thermodynamic, chemical kinetic and statistical considerations". In: *Combustion and Flame* 193 (2018), pp. 502–519.

[15] Takuma Sato, Stephen Voelkel, and Venkat Raman. "Detailed chemical kinetics based simulation of detonation-containing flows". In: *Turbo Expo: Power for Land, Sea, and Air*. Vol. 51050. American Society of Mechanical Engineers. 2018, V04AT04A063.

[16] Shivam Barwey and Venkat Raman. "A Neural Network-Inspired Matrix Formulation of Chemical Kinetics for Acceleration on GPUs". In: *Energies* 14.9 (2021), p. 2710.

[17] WE Ranz and WR Marshall. "Evaporation from droplets". In: *Chem. Eng. Prog* 48.3 (1952), pp. 141–146.

[18] R.S. Miller, K. Harstad, and J. Bellan. "Evaluation of equilibrium and non-equilibrium evaporation models for many-droplet gas-liquid flow simulations". In: *International Journal of Multiphase Flow* 24.6 (1998), pp. 1025–1055. ISSN: 0301-9322.




**Distribution Statement A: Approved for Public Release; Distribution is Unlimited. AFRL-2021-2661.**